New Journal of Physics
The open access journal at the forefront of physics

Deutsche Physikalische Gesellschaft DPG IOP Institute of Physics

OPEN ACCESS

Additional boundary conditions for nonconnected wire media

To cite this article: Mário G Silveirinha 2009 *New J. Phys.* **11** 113016

View the article online for updates and enhancements.

You may also like

- The hybrid absorbing boundary condition for one-step extrapolation and its application in wavefield decomposition-based reverse time migration
Enjiang Wang and Yang Liu
- Probability of boundary conditions in quantum cosmology
Yasusada Nambu and Hiroshi Suenobu
- Boundary condition influences on the effective area of a local heat flux probe
R S Figliola and M Swaminathan

This content was downloaded from IP address 193.137.201.233 on 21/11/2023 at 11:33

New Journal of Physics
The open-access journal for physics

Additional boundary conditions for nonconnected wire media

Mário G Silveirinha
University of Coimbra, Department of Electrical Engineering-Instituto de Telecomunicações, 3030 Coimbra, Portugal
E-mail: mario.silveirinha@co.it.pt

New Journal of Physics **11** (2009) 113016 (27pp)
Received 31 July 2009
Published 10 November 2009
Online at http://www.njp.org/
doi:10.1088/1367-2630/11/11/113016

Abstract. Continuing our recent work (2008 *New J. Phys.* **10** 053011), we demonstrate that due to strong nonlocal effects additional boundary conditions (ABCs) are essential to characterize the reflection of electromagnetic waves by nonconnected wire arrays using homogenization methods. Based on simple physical considerations, we derive the ABCs for circumstances where the wire medium is adjacent either to a dielectric or to a conducting material, and demonstrate that in the lossless case such boundary conditions ensure the conservation of the power flow. It is shown that the number of ABCs is related to the number of metallic wires in a unit cell. We illustrate the application of the novel boundary conditions to several configurations with practical interest.

© IOP Publishing Ltd and Deutsche Physikalische Gesellschaft

Contents

1. Introduction

Artificial materials formed by long metallic wires have attracted significant attention in recent years [1]–[14]. In some circumstances such wire media may be characterized by a plasmonic-type electric response, which potentially may enable interesting phenomena to occur such as superlensing [15], negative refraction [12, 13] or the excitation of strongly localized electromagnetic modes. However, it has been known for some time that in general wire media may fail to completely mimic the properties of a local plasma, and may have a spatially dispersive response [4, 6], [16]–[22], i.e. the electric displacement vector in a given point of space cannot be written exclusively in terms of the macroscopic field at the considered point, but, on the contrary, may depend on the distribution of the electric field in a neighborhood that encompasses many unit cells. This property is a consequence of the fact that the metallic wires are spanned over many unit cells, and consequently the polarization acquired by the metallic inclusions in a given unit cell (which is roughly proportional to the current along the wires), may depend significantly on the electric field outside the considered cell. Recently, it was suggested that the spatial dispersion effects may be reduced either by attaching conducting structures on the wires or by coating the wires with a magnetic material [23]. In [15], it was also demonstrated that at infrared and optical frequencies the nonlocal effects may be significantly weakened when the radius of the metallic rods is comparable to (or smaller than) the skin depth of the metal.

Even though in some applications spatial dispersion effects may be regarded as undesirable, in other circumstances they may open new possibilities. For example, in part due to nonlocal effects, an array of parallel wires may behave as a material with extreme optical anisotropy and this may enable the transport and manipulation of the near-field [7], [9]–[11], [24, 25]. Moreover, in a recent series of works it was shown that the spatially dispersive properties of a crossed wire mesh may enable the realization of materials with an extreme index of refraction [14], the realization of ultra-subwavelength waveguides [14, 26], superlensing [27],

broadband all-angle negative refraction [28], and low-loss broadband anomalous dispersion [29]. Some of these effects (e.g. the low-loss anomalous spectral dispersion) are specific to spatially dispersive materials, and cannot be observed in local materials. Due to these and other potential applications, the accurate characterization and modeling of nonlocal materials gain in importance.

One of the peculiarities of nonlocal materials is that they may support additional waves, i.e. for a fixed direction of propagation and a fixed frequency, the number of plane waves supported by the material may be greater than two, differing in this way from conventional local materials. For example, some of the plane waves may have identical polarization (i.e. the same orientation for the electric field) and be associated with different wave vectors. It is well known that such property implies that the classical boundary conditions, which impose the continuity of the tangential components of the electric and magnetic fields, may be insufficient to solve a scattering problem at an interface between a spatially dispersive material and another material, due to the degrees of freedom associated with the 'new' waves. A possible strategy to overcome this problem is the introduction of additional boundary conditions (ABCs) [30]–[33]. In [5, 34], alternative 'ABC-free' strategies are described.

There is no general theory for the derivation of ABCs. In fact, the ABCs depend on the very specific microstructure of the material, and should describe the dynamics of the internal variables of the nonlocal material, so that the degrees of freedom are removed. In recent works, the ABC approach was successfully used to model the reflection and refraction of electromagnetic waves at an interface between a wire medium formed by parallel wires and a conventional (dielectric or conducting) material [35, 36].

The objective of this paper is to generalize the theory of our previous works [35, 36] to the case of nonconnected 'double' and 'triple' wire media, and demonstrate that the introduction of suitable ABCs enables the accurate modeling of these structures using homogenization techniques. As mentioned before, such materials may have interesting applications to several problems [14], [26]–[29], which justifies, besides obvious theoretical motivations, the present study. It should be mentioned that it is not trivial to extend the theory of [35, 36] to the case of more complex metamaterial topologies. For example, it will be shown here that in general at an interface between a crossed wire mesh and a regular dielectric two distinct ABCs are required, whereas for an array of parallel wires one single ABC is sufficient to characterize the interface effects [35, 36].

This paper is organized as follows. In section 2, we derive the ABCs. In section 3, it is demonstrated that in the lossless case the proposed ABCs ensure the conservation of the power flow through a wire medium slab. A formula for the Poynting vector in the spatially dispersive material is derived. Then, in sections 4–6, we illustrate the application of the ABCs in several scenarios of interest, and demonstrate their accuracy using full-wave numerical simulations. In particular, we discuss the potentials of a wire mesh in the realization of ultra-subwavelength waveguides and the emergence of negative refraction. Finally, in section 7 the conclusions are drawn. It is assumed that the fields are monochromatic and have the time dependence $e^{-i\omega t}$.

In this work, we use several different notations for the field entities. For the convenience of the reader, the meaning of these notations is summarized below for the electric field case:

- **e**: microscopic electric field. This is the exact solution of the Maxwell's equations, taking into account the exact microstructure of the material.
- **E**: 'bulk' electric field. This is the electric field that results from the homogenization of the bulk material. Specifically, the macroscopic field is obtained by averaging the microscopic

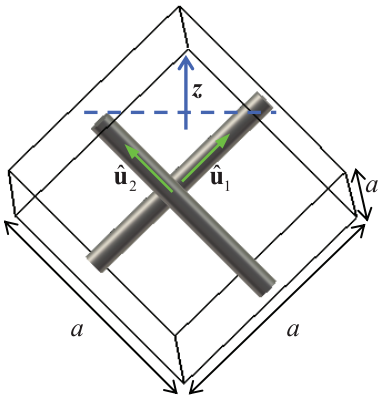

Figure 1. Geometry of the unit cell of the 'bulk' double wire medium ($N = 2$). The cubic unit cell contains two nonconnected metallic wires. The dashed line represents a hypothetical cut of the bulk material with a plane normal to the z-direction.

field over a volumetric region within which the structure is invariant to translations along three independent directions of space.

- $\mathbf{E}_{\mathrm{av,T}}$: transverse-averaged electric field. This definition assumes that the considered structure is periodic along two directions of space (assumed parallel to the xoy plane). However, the periodicity along z is not required. The transverse-averaged field is obtained by averaging the microscopic field exclusively along the directions parallel to the xoy plane, as detailed in section 2.

2. Derivation of the ABCs

Here, we generalize the ideas of [35, 36] and derive ABCs that enable the characterization of the internal variables responsible for the spatial dispersion effects in nonconnected wire media.

The material is formed by N mutually orthogonal and nonconnected sets of wires, oriented along the directions of space $\hat{\mathbf{u}}_n$ $(n = 1, \ldots, N)$ [18], where $N = 1, 2, 3$ is the number of components of the wire medium. Each wire array is arranged in a square lattice with lattice constant a. The radius of the wires is r_{w}. For $N = 1$, the material consists of a single array of parallel wires, and for $N = 2$ ($N = 3$) it is formed by a double (triple) wire array. The distance between adjacent orthogonal wires is $a/2$. It is assumed that the wires are good conductors, i.e. the radius of the wires is much larger than the skin depth of metal at the frequency of operation. For reasons that will be clear shortly, in general the unit vectors $\hat{\mathbf{u}}_n$ are not oriented along the coordinate axes x, y and z.

As an example, the unit cell of the bulk double wire medium (crossed wire mesh) is represented in figure 1. The unbounded material is formed by the periodic repetition of the primitive cell. Since the wires intersect the boundaries of the unit cell, it should be clear that such construction effectively yields infinitely long wires.

Let us suppose that the bulk material is sliced to form a planar interface with another adjacent material (a regular dielectric or metal; see figure 4(c)). This operation breaks the translational symmetry of the system along the direction normal to the interface, which without

loss of generality is assumed to be the z-axis. In particular, the wires lying in cells of the wire medium adjacent to the interface are sliced as well (except, possibly, if some of the wires are parallel to the interface). However, the periodicity of the system in the transverse plane (xoy-plane) is preserved.

We use the transverse-average (TA) field approach introduced in [37], in order to describe the electromagnetic wave propagation using homogenization methods. The TA fields are obtained by averaging the 'microscopic' fields over the directions parallel to the interface (x- and y-directions), i.e. over the directions along which the system has translational symmetry. It is assumed that the microscopic fields have the Floquet–Bloch property in the xoy-plane, being characterized by the transverse wave vector $\mathbf{k}_\parallel = (k_x, k_y, 0)$. This situation occurs, for example, when the wire medium slab is illuminated by a plane wave, being in such circumstances $\mathbf{k}_\parallel$ determined by the direction of incidence and by the frequency of operation.

Following [37], the TA-electric and induction fields are defined as

$$\begin{aligned}\mathbf{E}_{\mathrm{av,T}}(z) &= \frac{1}{A_{\mathrm{cell}}}\int_{\Omega_\mathrm{T}} \mathbf{e}(\mathbf{r})\mathrm{e}^{-\mathrm{i}\mathbf{k}_\parallel\cdot\mathbf{r}}\mathrm{d}x\mathrm{d}y,\\ \mathbf{B}_{\mathrm{av,T}}(z) &= \frac{1}{A_{\mathrm{cell}}}\int_{\Omega_\mathrm{T}} \mathbf{b}(\mathbf{r})\mathrm{e}^{-\mathrm{i}\mathbf{k}_\parallel\cdot\mathbf{r}}\mathrm{d}x\mathrm{d}y,\end{aligned} \tag{1}$$

where $\mathbf{e}$ and $\mathbf{b}$ are the microscopic electric and induction fields, Ω_T represents the transverse unit cell in each $z = \text{const.}$ plane and A_{cell} is the area of Ω_T. As demonstrated in [37], the TA fields verify the differential system (assuming the time convention $\mathrm{e}^{-\mathrm{i}\omega t}$):

$$\begin{aligned}\left(\mathrm{i}\mathbf{k}_\parallel + \frac{\mathrm{d}}{\mathrm{d}z}\hat{\mathbf{u}}_z\right)\times\frac{\mathbf{B}_{\mathrm{av,T}}}{\mu_0} &= -\mathrm{i}\omega\varepsilon_0\varepsilon_\mathrm{h}\mathbf{E}_{\mathrm{av,T}} + \mathbf{J}_{d,\mathrm{av}},\\ \left(\mathrm{i}\mathbf{k}_\parallel + \frac{\mathrm{d}}{\mathrm{d}z}\hat{\mathbf{u}}_z\right)\times\mathbf{E}_{\mathrm{av,T}} &= \mathrm{i}\omega\mathbf{B}_{\mathrm{av,T}},\end{aligned} \tag{2}$$

where ε_h is the relative permittivity of the host medium, and $\mathbf{J}_{d,\mathrm{av}}$ is the averaged microscopic current. It should be clear that the TA fields depend exclusively on the z coordinate.

For the considered wire media, formed by metallic inclusions, the averaged microscopic current is given by [37]:

$$\mathbf{J}_{d,\mathrm{av}}(z) = \frac{1}{A_{\mathrm{cell}}}\int_{\partial A(z)} \mathbf{J}_\mathrm{c}(\mathbf{r})\mathrm{e}^{-\mathrm{i}\mathbf{k}_\parallel\cdot\mathbf{r}}\frac{1}{|\hat{\nu}\times\hat{\mathbf{u}}_z|}\mathrm{d}l, \tag{3}$$

where $\mathbf{J}_\mathrm{c} = \hat{\nu}\times\mathbf{b}/\mu_0$ is the density of electric current on the surface of a given wire, $\hat{\nu}$ is the unit vector normal to the surface of the wire, $\partial A(z)$ is the contour determined by the intersection of the surface of the wires in the unit cell and the pertinent $z = \text{const.}$ plane, and $\mathrm{d}l$ is the element of arc. Strictly speaking formula (3) is only valid when there are no wires parallel to the transverse plane (otherwise the integrand becomes singular), which is the case of interest in this work. The key result is that, similar to the analysis of [36], it is possible to write $\mathbf{J}_{d,\mathrm{av}}$ in terms of the microscopic electric currents induced on the metallic wires.

Indeed, assuming that the wires are relatively thin, $r_\mathrm{w} \ll a$, it is a good approximation to consider that the density of current over the nth wire in the unit cell (parallel to the unit vector $\hat{\mathbf{u}}_n$) is of the form (thin wire approximation):

$$\mathbf{J}_\mathrm{c}|_{\partial D_n} = \frac{I_n(z)}{2\pi r_\mathrm{w}}\mathrm{e}^{+\mathrm{i}\mathbf{k}_\parallel\cdot\mathbf{r}}\hat{\mathbf{u}}_n, \tag{4}$$

where ∂D_n represents the surface of the considered wire, I_n is the electric current, and $n = 1, \ldots, N$, where N is the number of components of the wire medium. Note that the density of current is modulated by the exponential factor $e^{+i\mathbf{k}_\parallel \cdot \mathbf{r}}$, because of the assumed Floquet periodicity of the microscopic fields in the transverse plane. Substituting equation (4) into equation (3), it may be shown that the averaged microscopic current is given by

$$\mathbf{J}_{d,\mathrm{av}}(z) = \frac{1}{a^2} \sum_n I_n(z) \hat{\mathbf{u}}_n. \tag{5}$$

Thus $\mathbf{J}_{d,\mathrm{av}}$ has indeed a simple relation with the microscopic electric currents. On the other hand, from equation (2) it is straightforward to write the averaged current as a function of the macroscopic TA-electric field

$$\mathrm{i}\omega\mu_0 \mathbf{J}_{d,\mathrm{av}}(z) = \left(\mathrm{i}\mathbf{k}_\parallel + \frac{\mathrm{d}}{\mathrm{d}z}\hat{\mathbf{u}}_z\right)\left(\mathrm{i}\mathbf{k}_\parallel + \frac{\mathrm{d}}{\mathrm{d}z}\hat{\mathbf{u}}_z\right)\mathbf{E}_{\mathrm{av,T}} + \left(k_\parallel^2 - \left(\frac{\omega}{c}\right)^2 \varepsilon_\mathrm{h} - \frac{\mathrm{d}^2}{\mathrm{d}z^2}\right)\mathbf{E}_{\mathrm{av,T}}. \tag{6}$$

Equations (5) and (6) establish the connection between the microscopic currents and the macroscopic electric field and will be used in what follows to derive ABCs for nonconnected wire media.

Let us consider first the case where the material adjacent to the wire medium is nonconducting (e.g. a dielectric). In this situation, similar to the case of an array of parallel wires [35, 36], the microscopic electric current must vanish at the interface. This means that $I_n = 0$, $n = 1, \ldots, N$, at the interface with the dielectric material, i.e. the currents associated with different wires in the unit cell must vanish independently. But, equation (5) shows that this property implies that the averaged current verifies

$$\mathbf{J}_{d,\mathrm{av}} \cdot \hat{\mathbf{u}}_n = 0, \quad \text{(dielectric interface)}, \quad n = 1, \ldots, N. \tag{7}$$

This equation, along with equation (6), may be regarded as a set of N-independent ABCs at the interface with the dielectric material. It should be clear that equation (7) may be written exclusively in terms of the macroscopic electric field and its derivatives, and that the number of ABCs is equal to the number of metallic wires in a unit cell ($N = 2$ for the double wire medium and $N = 3$ for the triple wire medium). Obviously, equation (7) assumes that all the metallic wires intersect the interface. When some $\hat{\mathbf{u}}_n$ is parallel to the interface, in general $\mathbf{J}_{d,\mathrm{av}} \cdot \hat{\mathbf{u}}_n$ does not vanish at the interface because the path of the current is not interrupted.

The ABCs (7) are a generalization of the results of our previous works [35, 36] for an array of parallel wires ($N = 1$). As demonstrated in [35, 36], when $N = 1$ the ABC and the classical boundary conditions imply the continuity of the normal component of the electric field multiplied by the host permittivity at the interface. In particular, when the host material is air, the ABC, together with the classical boundary conditions, is equivalent to the continuity of all the Cartesian components of the electromagnetic field. Interestingly, when $N = 2$ or 3 the situation is quite different, specifically, since the number of ABCs is greater than one, the continuity of the normal component of the electric field multiplied by the host permittivity (one single independent equation) cannot be regarded as equivalent to all the ABCs (two or three independent equations).

Another case of interest occurs when the material adjacent to the wire medium has very high conductivity (e.g. a metal). It is obvious that in such configuration the ABCs (7) are not valid, because, assuming that the wires are connected with good Ohmic contact to the ground

plane, the current path is not interrupted at the interface. In fact, it was demonstrated in [36] that it is the microscopic electric density of charge σ_c that vanishes at the connection point with the metallic surface, rather than the electric current. Thus, electric charge cannot be accumulated at the connection points between the wires and the ground plane. For a wire directed along the nth direction, the condition $\sigma_c = 0$ is equivalent to $\frac{dJ_{c,n}}{ds} = 0$, where $J_{c,n} = \frac{I_n(z)}{2\pi r_w} e^{+i\mathbf{k}_\parallel \cdot \mathbf{r}}$ is the density of current along the considered wire (see equation (4)), and s is a coordinate measured along the wire axis. It is clear that for the nth wire $\frac{d}{ds} = \hat{\mathbf{u}}_n \cdot \nabla$, and hence the condition $\frac{dJ_{c,n}}{ds} = 0$ is equivalent to $\hat{\mathbf{u}}_n \cdot (i\mathbf{k}_\parallel + \hat{\mathbf{u}}_z \frac{d}{dz}) I_n(z) = 0$. Thus, using equation (5), it is readily found that the averaged current must verify

$$\left(i\mathbf{k}_\parallel + \hat{\mathbf{u}}_z \frac{d}{dz}\right) \cdot \hat{\mathbf{u}}_n \hat{\mathbf{u}}_n \cdot \mathbf{J}_{d,\mathrm{av}} = 0, \quad \text{(metallic interface)}, \quad n = 1, \ldots, N. \tag{8}$$

The above equations define a set of N-independent ABCs at the interface between a nonconnected wire medium and a ground plane, and are a generalization of the results of [36]. Again, it should be clear that equations (6) and (8) define a functional relation between the macroscopic electric field and its derivatives at the interface, and that it is implicit that all the wires intersect the interface.

The application of the proposed ABCs will be illustrated in sections 5 and 6, where, for the case of a double wire medium, it is shown with full-wave simulations that the ABCs may enable the accurate analytical modeling of wave propagation.

An important point, which is discussed next, is the characterization the TA-macroscopic fields in the wire medium. The obvious idea is to write the macroscopic fields in the material as a superposition of plane waves. The plane waves may be characterized using the homogenization model proposed in [14, 18, 19]. Specifically, the dielectric function of the nonconnected wire medium is

$$\begin{aligned} \bar{\bar{\varepsilon}}(\omega, \mathbf{k}) &= \varepsilon_h \bar{\bar{\mathbf{I}}} + \sum_{n=1}^{N} \left(\varepsilon_{n,n}(\omega, \mathbf{k}) - \varepsilon_h\right) \hat{\mathbf{u}}_n \hat{\mathbf{u}}_n, \\ \varepsilon_{n,n}(\omega, \mathbf{k}) &= \varepsilon_h \left(1 + \frac{1}{\frac{1}{f_V(\varepsilon_m/\varepsilon_h - 1)} - \frac{(\omega/c)^2 \varepsilon_h - k_n^2}{\beta_p^2}}\right), \end{aligned} \tag{9}$$

where $\bar{\bar{\mathbf{I}}}$ is the identity dyadic, $\hat{\mathbf{u}}_n \hat{\mathbf{u}}_n = \hat{\mathbf{u}}_n \otimes \hat{\mathbf{u}}_n$ represents the dyadic (tensor) product of two vectors, $\beta_p = [2\pi/(\ln(a/2\pi r_w) + 0.5275)]^{1/2}/a$ is the plasma wavenumber, $f_V = \pi(r_w/a)^2$, ε_h is the host relative permittivity, $\varepsilon_m = \varepsilon_m(\omega)$ is the metal relative complex permittivity, c is the speed of light in vacuum, $\mathbf{k} = (k_x, k_y, k_z)$ is the wave vector, and $k_n = \mathbf{k} \cdot \hat{\mathbf{u}}_n$.

Using the dielectric function (9) it is possible to calculate the *bulk* macroscopic fields $(\mathbf{E}, \mathbf{B})$. An important observation is that, for a general metamaterial, the bulk macroscopic fields may not be coincident with the TA fields used in the formulation of the ABCs (7) and (8). Indeed, the bulk macroscopic fields, as defined in [18, 37], are obtained by averaging the microscopic fields over the unit cell (a volumetric region) of the periodic material, whereas the TA fields are obtained by averaging the microscopic fields over the transverse unit cell (a surface) [37]. Fortunately, as demonstrated in appendix A for nonconnected wire media, and supposing that all the wires intersect the interface (i.e. there are no wires parallel to the interface), it is possible to identify to a very good approximation the bulk macroscopic fields with the TA fields. This

means that it is possible to drop the subscripts 'av, T' in equation (6), and characterize the TA-field $\mathbf{E}_{\mathrm{av,T}}$ using the dielectric function of the bulk material. These ideas are further clarified in sections 5 and 6.

3. Conservation of the power flow

An important question that may be formulated is whether in the lossless case (i.e. when both ε_{h} and ε_{m} are real valued) the proposed ABCs ensure the conservation of the power flow in the wire medium. We demonstrate that that is indeed the case. The theory developed below is based on the bulk medium fields, which as mentioned in the end of the previous section, may be regarded as equivalent to the transverse-averaged fields in the case of interest.

Let $(\mathbf{E}, \mathbf{H})$ be a solution of Maxwell's equations in the homogenized bulk wire medium such that the variation in the x- and y-coordinates is of the form $\mathrm{e}^{\mathrm{i}\mathbf{k}_{\parallel}\cdot\mathbf{r}}$, with $\mathbf{k}_{\parallel} = (k_x, k_y, 0)$ a real-valued vector. The bulk magnetic field is by definition $\mathbf{H} = \mathbf{B}/\mu_0$. Thus, $(\mathbf{E}, \mathbf{H})$ verify

$$\begin{aligned} \nabla \times \mathbf{H} &= -\mathrm{i}\omega\mathbf{D}, \\ \nabla \times \mathbf{E} &= \mathrm{i}\omega\mu_0\mathbf{H}, \end{aligned} \tag{10}$$

where $\mathbf{D} = \varepsilon_0\varepsilon_{\mathrm{h}}\mathbf{E} + \mathbf{P}$ is the electric displacement vector in the spatially dispersive material and $\mathbf{P}$ is the nonlocal (generalized) polarization vector (relative to the host material). Let us define $\mathbf{S}^0$ as follows:

$$\mathbf{S}^0 = \tfrac{1}{2}\mathrm{Re}\,\{\mathbf{E} \times \mathbf{H}^*\}. \tag{11}$$

It is well known that in general $\mathbf{S}^0$ cannot be identified with the Poynting vector in a spatially dispersive material [38, 39]. In fact, there is no general formula for the Poynting vector in a spatially dispersive material. The only circumstances in which the Poynting vector is actually known is when the material is lossless and the electromagnetic field is associated with a propagating plane wave [39]. In what follows, we will demonstrate that for lossless nonconnected wire media, it is possible to define unambiguously the z-component of the Poynting vector, even if the electromagnetic field has an arbitrary variation with z (not necessarily a propagating plane wave).

To begin with, we note that from equation (10) it follows that

$$\nabla \cdot \mathbf{S}^0 = \tfrac{1}{2}\mathrm{Re}\,\{-\mathrm{i}\omega\mathbf{E}\cdot\mathbf{D}^*\} = \tfrac{1}{2}\mathrm{Re}\,\{-\mathrm{i}\omega\mathbf{E}\cdot\mathbf{P}^*\}, \tag{12}$$

where the second identity is a consequence of the fact that the host permittivity ε_{h} is a real number in the absence of loss. The next step is to relate $\mathbf{P}$ and $\mathbf{E}$. In the spectral (Fourier) domain we clearly have that

$$\tilde{\mathbf{P}}(\mathbf{k}) = \varepsilon_0\left(\bar{\bar{\varepsilon}}(\omega, \mathbf{k}) - \varepsilon_{\mathrm{h}}\bar{\bar{\mathbf{I}}}\right)\cdot\tilde{\mathbf{E}}(\mathbf{k}), \tag{13}$$

where $\bar{\bar{\varepsilon}}$ is the relative permittivity of the wire medium, the symbol '$\sim$' denotes the spatial Fourier transform, and here $\mathbf{k}$ represents the Fourier coordinates. In particular, the projections of $\tilde{\mathbf{E}}$ and $\tilde{\mathbf{P}}$ onto the principal direction $\hat{\mathbf{u}}_n$ of the dielectric function verify $\tilde{P}_n = \varepsilon_0(\varepsilon_{n,n}(\omega, k_n) - \varepsilon_{\mathrm{h}})\tilde{E}_n$ with $k_n = \mathbf{k}\cdot\hat{\mathbf{u}}_n$ $(n = 1, \ldots, N)$. Thus, using equation (9) it follows that

$$\tilde{E}_n = \frac{1}{\varepsilon_0\varepsilon_{\mathrm{h}}\beta_{\mathrm{p}}^2}\left(k_n^2 - \frac{\omega^2}{c^2}\varepsilon_{\mathrm{h}} + \frac{\beta_{\mathrm{p}}^2}{f_{\mathrm{V}}\,(\varepsilon_{\mathrm{m}}/\varepsilon_{\mathrm{h}} - 1)}\right)\tilde{P}_n. \tag{14}$$

Hence, calculating the inverse Fourier transform, we obtain the following relation in the space domain:

$$E_n = \frac{1}{\varepsilon_0 \varepsilon_h \beta_p^2}\left[\left(-i\hat{\mathbf{u}}_n \cdot \nabla\right)^2 - \frac{\omega^2}{c^2}\varepsilon_h + \frac{\beta_p^2}{f_V\left(\varepsilon_m/\varepsilon_h - 1\right)}\right] P_n. \tag{15}$$

But, since it is assumed that the variation of the electromagnetic field in the x- and y-coordinates is of the form $e^{i\mathbf{k}_\parallel \cdot \mathbf{r}}$, we have that $-i\hat{\mathbf{u}}_n \cdot \nabla = \hat{\mathbf{u}}_n \cdot \mathbf{k}_\parallel - i\hat{\mathbf{u}}_n \cdot \hat{\mathbf{u}}_z \frac{d}{dz}$. Thus, after some simplifications, it is found that

$$\mathrm{Re}\left\{-iP_n^* E_n\right\} = \frac{1}{\varepsilon_0 \varepsilon_h \beta_p^2}\mathrm{Re}\left\{i\left(\hat{\mathbf{u}}_n \cdot \hat{\mathbf{u}}_z\right)^2 P_n^* \frac{d^2 P_n}{dz^2} - 2\left(\mathbf{k}_\parallel \cdot \hat{\mathbf{u}}_n\right)\left(\hat{\mathbf{u}}_n \cdot \hat{\mathbf{u}}_z\right) P_n^* \frac{dP_n}{dz}\right\}. \tag{16}$$

Next, we note that

$$\mathrm{Re}\left\{iP_n^* \frac{d^2 P_n}{dz^2}\right\} = \mathrm{Re}\left\{\frac{d}{dz}\left(iP_n^* \frac{dP_n}{dz}\right)\right\}$$

and that

$$\mathrm{Re}\left\{P_n^* \frac{dP_n}{dz}\right\} = \frac{d}{dz}\left(\frac{|P_n|^2}{2}\right)$$

to finally write

$$\mathrm{Re}\left\{-iP_n^* E_n\right\} = \frac{1}{\varepsilon_0 \varepsilon_h \beta_p^2}\frac{d}{dz}\mathrm{Re}\left\{\left(\hat{\mathbf{u}}_n \cdot \hat{\mathbf{u}}_z\right)^2 iP_n^* \frac{dP_n}{dz} - \left(\mathbf{k}_\parallel \cdot \hat{\mathbf{u}}_n\right)\left(\hat{\mathbf{u}}_n \cdot \hat{\mathbf{u}}_z\right)|P_n|^2\right\}. \tag{17}$$

We are now in a position to calculate the divergence of $\mathbf{S}^0$, given by equation (12). On one hand, we note that due to the assumed dependence of $(\mathbf{E}, \mathbf{H})$ in the x- and y-coordinates, it is clear that $\mathbf{S}^0$ depends exclusively on z, and thus $\nabla \cdot \mathbf{S}^0 = \frac{dS_z^0}{dz}$ where S_z^0 is the z-component of $\mathbf{S}^0$. On the other hand, it is obvious that $\mathbf{P}^* \cdot \mathbf{E} = \sum_{n=1}^N P_n^* E_n$ because the only nonvanishing components of $\mathbf{P}$ are precisely the P_ns (remember also that the unit vectors $\hat{\mathbf{u}}_n$ are mutually orthogonal). Therefore equations (12) and (17) show that

$$\frac{dS_z}{dz} = 0, \tag{18}$$

where S_z is given by

$$S_z = S_z^0 - \frac{\omega}{2}\frac{1}{\varepsilon_0 \varepsilon_h \beta_p^2}\mathrm{Re}\left\{i\sum_{n=1}^N \hat{\mathbf{u}}_n \cdot \hat{\mathbf{u}}_z P_n^* \left(i\mathbf{k}_\parallel + \frac{d}{dz}\hat{\mathbf{u}}_z\right) \cdot \hat{\mathbf{u}}_n P_n\right\}. \tag{19}$$

As discussed below, S_z is the z-component of the Poynting vector in the spatially dispersive material. Before that discussion, let us show that the conservation law (18) implies that the ABCs introduced in this work guarantee the conservation of power flow at an interface with a dielectric or a metallic material.

Indeed, it is clear from equation (19) that at the points z such that for every $n = 1, \ldots, N$,

$$\text{either } P_n = 0 \quad \text{or} \quad \left(i\mathbf{k}_\parallel + \frac{d}{dz}\hat{\mathbf{u}}_z\right) \cdot \hat{\mathbf{u}}_n P_n = 0, \tag{20}$$

we have that $S_z = S_z^0$. Comparing equations (2) with (10), and using the fact that in the nonconnected wire medium the bulk medium fields can be identified with the TA fields (see appendix A), it is evident that the polarization vector verifies,

$$\mathbf{P} = \frac{1}{-\mathrm{i}\omega}\mathbf{J}_{d,\mathrm{av}}\mathrm{e}^{\mathrm{i}\mathbf{k}_\parallel\cdot\mathbf{r}}, \tag{21}$$

where $\mathbf{J}_{d,\mathrm{av}}$ is the averaged microscopic current. But then it follows that the first condition in equation (20) is equivalent to the ABC (7), whereas the second condition is equivalent to the ABC (8). Hence, we conclude that at the points z of the material where either the ABCs (7) (associated with dielectric interfaces) or the ABCs (8) (associated with metallic interfaces) are enforced, we have that $S_z = S_z^0$.

Let us now consider a truncated wire medium (wire medium slab) with interfaces at $z = z_i$ and $z = z_f$. From equation (18) we see that in the lossless case S_z is constant inside the wire medium, and consequently when the ABCs are enforced S_z^0 has the same value at the two interfaces: $S_z^0(z_i) = S_z^0(z_f)$ (calculated from the wire medium side). But due to the classical boundary conditions (continuity of the tangential components of $\mathbf{E}$ and $\mathbf{H}$ at the interfaces), S_z^0 may be evaluated either at the wire medium side of the interface or at the exterior side with the same result. Thus, we have demonstrated that the proposed ABCs together with the classical boundary conditions imply that $S_z^0(z_i) = S_z^0(z_f)$, being S_z^0 evaluated at the exterior side of the interface, where it is obviously the z-component of the Poynting vector. This shows that in the lossless case the ABCs (7) and (8) (or more generally the condition (20)) guarantee, in fact, the conservation of the power flow through a wire medium slab, as we wanted to prove. This result is valid for simple ($N = 1$), double ($N = 2$) or triple ($N = 3$) wire media.

To show that S_z can be identified with the z-component of the Poynting vector in the spatially dispersive material, we consider the typical case where the electromagnetic field is a superposition of plane waves:

$$\mathbf{E}(\mathbf{r}) = \sum_l \mathbf{E}_l \mathrm{e}^{+\mathrm{i}\mathbf{k}_l\cdot\mathbf{r}}, \tag{22}$$

where $\mathbf{E}_l$ is a constant vector (determines the polarization of the plane wave), and $\mathbf{k}_l = \mathbf{k}_\parallel + k_z^{(l)}\hat{\mathbf{u}}_z$ is the wave vector associated with the plane wave. The z-component $k_z^{(l)}$ may be either real (positive or negative) or complex valued (as discussed in section 4, the wire medium may support evanescent modes even in the absence of loss). It is supposed that each individual plane wave verifies equations (10). In appendix B, we demonstrate that for such superposition of plane waves, S_z, defined by (19), may be rewritten as

$$S_z = \sum_{\substack{l,m \\ \mathbf{k}_l = \mathbf{k}_m^*}} \mathrm{Re}\left\{\left(\frac{1}{2}\mathbf{E}_l \times \mathbf{H}_m^*\right)\cdot\hat{\mathbf{u}}_z - \frac{\omega\varepsilon_0}{4}\mathbf{E}_m^*\cdot\frac{\partial\bar{\bar{\varepsilon}}\,(\omega,\mathbf{k}_l)}{\partial k_z}\cdot\mathbf{E}_l\right\}, \tag{23}$$

where the summation is restricted to the indices l, m so that $\mathbf{k}_l = \mathbf{k}_m^*$, and $\mathbf{H}_l$ is the magnetic field associated with $\mathbf{E}_l$. But for a single plane wave with a real wave vector the above formula reduces to the well-known expression of the Poynting vector in a general spatially dispersive material [38, 39]. This demonstrates that S_z may indeed be identified with the z-component of the Poynting vector. It should however be stressed that the above formula is more general than the results reported in [38, 39], which apply exclusively to a single plane wave with a real wave vector. The result (23) generalizes the classical result to the case of a superposition of plane waves (possibly associated with complex wave vectors) in a lossless nonconnected wire medium.

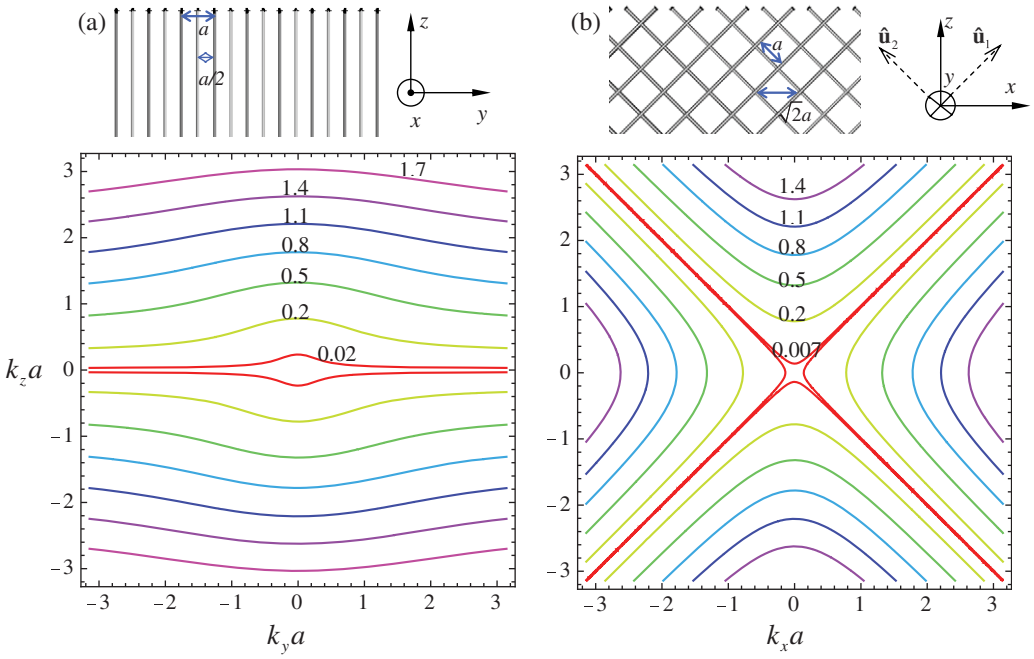

Figure 2. Isofrequency contours of the fundamental plane wave mode for (a) propagation in the yoz-plane with the electric field along the x-direction; (b) propagation in the xoz-plane with the electric field in the same plane. The radius of the wires is $r_w = 0.05a$ and the metal is assumed to be a perfect conductor. The text insets indicate the value of the normalized frequency $\omega a/c$.

4. Crossed wire mesh

In the rest of the paper, we apply the developed theory to the particular case of a crossed wire mesh formed by a double array of metallic wires [6, 14, 19]. It is assumed that the wires are parallel to the xoz-plane, and that $\hat{\mathbf{u}}_1 = (1, 0, 1)/\sqrt{2}$ and $\hat{\mathbf{u}}_2 = (-1, 0, 1)/\sqrt{2}$. Thus, the angle of the wire axes with respect to the interface normal is $\pm 45^\circ$. A cut of the considered structure in the planes yoz and xoz is represented in figure 2. We will analyze the scattering and guiding of electromagnetic waves by the wire medium slab in the cases where the wave vector is confined to one of these two planes. Moreover, in case of propagation in the yoz-plane with will assume that the electric field is polarized along the x-direction, whereas in case of propagation in the xoz-plane we will restrict our attention to the situation where the magnetic field is along the y-direction (thus, in both cases, the electric field is in the xoz-plane).

Before addressing the problem of propagation in a finite structure (wire medium slab), next we will briefly review some key properties of the electromagnetic modes in the unbounded crossed wire mesh. Unlike a conventional local plasma, the metamaterial may support propagating modes for arbitrarily low frequencies [6, 8, 14, 18, 19]. Specifically, in the lossless case (e.g. for perfect electrical conductors (PEC), i.e. $\varepsilon_m = -\infty$), and for frequencies much lower than the effective plasma frequency, $\omega/c \ll \beta_p/\sqrt{\varepsilon_h}$, the wire medium supports a propagating plane wave with an electric field in the xoz-plane.

Following [14, 27], the plane waves supported by the material in the case of propagation in the yoz-plane ($k_x = 0$) with the electric field along the x-direction are characterized by the dispersion characteristic

$$\varepsilon(\omega, k_z)(\omega/c)^2 = k_y^2 + k_z^2, \quad \text{with} \quad \varepsilon(\omega, k_z) = \varepsilon_\mathrm{h}\left(1 + \frac{1}{\frac{1}{f_\mathrm{V}(\varepsilon_m/\varepsilon_\mathrm{h}-1)} - \frac{(\omega/c)^2\varepsilon_\mathrm{h} - k_z^2/2}{\beta_\mathrm{p}^2}}\right). \tag{24}$$

The isofrequency contours of the propagating mode are depicted in figure 2(a) for PEC wires with normalized radius $r_\mathrm{w}/a = 0.05$. Clearly, the material is strongly anisotropic, and the isofrequency contours resemble ellipses with a large axial ratio. It is seen that the contours are nearly perpendicular to the z-direction, and consequently the energy tends to flow along z. This suggests that adjacent wire planes tend to guide the wave along z, and obstruct the propagation along y. It was shown in [14] that the effective index of refraction for propagation along z is (assuming $\varepsilon_\mathrm{h} = 1$ and PEC wires):

$$n_\mathrm{ef} \equiv \left.\frac{k_z c}{\omega}\right|_{k_y=0} = \sqrt{\frac{3}{2} + \frac{1}{2}\left(1 + 8\left(\frac{\beta_\mathrm{p} c}{\omega}\right)^2\right)^{1/2}}. \tag{25}$$

Since $\beta_\mathrm{p} \sim 1/a$, one interesting feature of this structure is that for a fixed frequency the index of refraction may be greatly enhanced by reducing the spacing between the wires (maintaining the metal volume fraction) [14]. Other mechanisms to design materials with a high index were proposed in [40, 41], but the required microstructures are arguably much more complicated to fabricate than a crossed wire mesh.

As could be expected from the geometry of the material, the propagation properties in the xoz-plane ($k_y = 0$) are very different. The dispersion characteristic is now [28]

$$\frac{k_1^2}{k^2 - (\omega/c)^2\varepsilon_{11}} + \frac{k_2^2}{k^2 - (\omega/c)^2\varepsilon_{22}} = 1, \tag{26}$$

where $\varepsilon_{n,n}$ ($n = 1, 2$) is given by equation (9), $k^2 = k_x^2 + k_z^2$, and $k_n = \mathbf{k}\cdot\hat{\mathbf{u}}_n$, with $\mathbf{k} = (k_x, 0, k_z)$. The corresponding isofrequency contours are depicted in figure 2(b), and are two perpendicular hyperbolas. The electric field associated with each plane wave is nearly (but not exactly) tangent to the isofrequency contours [28]. The shape of the isofrequency contours suggests that propagation is favored along the coordinates axes, i.e. when the wave vector makes an angle of $\pm 45^\circ$ with the wire axes. On the other hand, when the wave vector is normal to one of wire axes the structure has a directional bandgap. The hyperbolic-shaped isofrequency contours may enable the emergence of negative refraction [6, 19, 28], as will be further discussed in section 6.

5. Propagation in the *yoz*-plane

In what follows, we apply the ABCs derived in section 2 to characterize the scattering of plane waves by a double-wire medium slab, assuming propagation in the yoz-plane (figure 2(a)). As in section 2, it is assumed that the normal to the interfaces is along the z-direction.

To begin with, we calculate the averaged microscopic current in the wire medium slab. It is assumed that the excitation is such that the electric field is along the x-direction. Clearly, for propagation in the yoz-plane the transverse wave vector is such that $\mathbf{k}_\parallel = k_y\hat{\mathbf{u}}_y$, where k_y is

determined by the excitation (for an incoming plane wave, $k_y = \omega/c \sin\theta_\mathrm{i}$ where θ_i is the angle of incidence). Thus, from equation (6), it is found that the averaged current verifies

$$\mathrm{i}\omega\mu_0 \mathbf{J}_{d,\mathrm{av}}(z) = \left(k_y^2 - \varepsilon_\mathrm{h}\frac{\omega^2}{c^2} - \frac{\mathrm{d}^2}{\mathrm{d}z^2}\right) E_x \hat{\mathbf{u}}_x, \tag{27}$$

where E_x is the electric field in the wire medium slab. The ABCs at a dielectric interface can now be easily obtained using equation (7). As discussed in section 2, in the double-wire medium case, one needs to impose two distinct ABCs at the interface ($N = 2$). However, in the present case the two ABCs (7) impose the same condition on the macroscopic electric field:

$$\frac{\mathrm{d}^2 E_x}{\mathrm{d}z^2} + \left(\varepsilon_\mathrm{h}\frac{\omega^2}{c^2} - k_y^2\right) E_x = 0 \quad \text{(dielectric interface)}. \tag{28}$$

This degeneracy occurs due to the exceptionally high symmetry of the system. In the general case, the ABCs are not redundant and yield, in fact, independent equations, as will be shown in section 6. Similarly, at a metallic interface, the two ABCs (8) also yield a single equation

$$\frac{\mathrm{d}^3 E_x}{\mathrm{d}z^3} + \left(\varepsilon_\mathrm{h}\frac{\omega^2}{c^2} - k_y^2\right) \frac{\mathrm{d}E_x}{\mathrm{d}z} = 0, \quad \text{(metallic interface)}. \tag{29}$$

Equations (28) and (29) correspond exactly to the ABCs that were enunciated in our previous works [14, 27] (with no proof). These ABCs can be readily applied to solve a scattering or wave-guiding problem when the wave vector is confined to the yoz-plane. Since the use of the ABCs for this specific configuration was already addressed in [14, 27], our discussion here will be somewhat abbreviated.

5.1. Slab standing in free-space

First, we consider the case where the wire medium slab stands in free space, and is illuminated by a plane wave characterized by the transverse wave number $k_y = \omega/c \sin\theta_\mathrm{i}$ (see the inset of figure 3). As mentioned in section 2, the key assumption is that the electromagnetic field inside the wire medium slab can be written as superposition of plane waves characterized by the dielectric function of the bulk (unbounded) material. Because of translational invariance k_y must be conserved, and thus the pertinent plane waves can be found from the solution of the dispersion characteristic (24) with respect to k_z, with ω and k_y determined by the excitation. As discussed in [14, 27], the solution of equation (24) yields exactly two different solutions for k_z^2. It should be clear that for a regular local dielectric slab there is only a single solution. This clarifies why for propagation in the yoz-plane, a single ABC is sufficient to characterize interface effects (despite that the wire medium has two components), i.e. since there is only one additional wave only one ABC is required. Thus, the electric field inside the metamaterial slab may be written as (the y dependence of the field is suppressed):

$$E_x = A_1^+ \mathrm{e}^{+\mathrm{i}k_{z,(1)}z} + A_1^- \mathrm{e}^{-\mathrm{i}k_{z,(1)}z} + A_2^+ \mathrm{e}^{+\mathrm{i}k_{z,(2)}z} + A_2^- \mathrm{e}^{-\mathrm{i}k_{z,(2)}z}, \tag{30}$$

where $k_{z,(i)} = k_{z,(i)}(\omega, k_y)$ are the solutions of the dispersion equation (24). As discussed in [14, 27], for long wavelengths and in the absence of loss, there is only a propagating mode in the wire medium, i.e. one of the propagation constants, let us say $k_{z,(1)}$, is real valued and is associated with the isofrequency contours depicted in figure 2(a), while the other propagation constant, $k_{z,(2)}$, is purely imaginary.

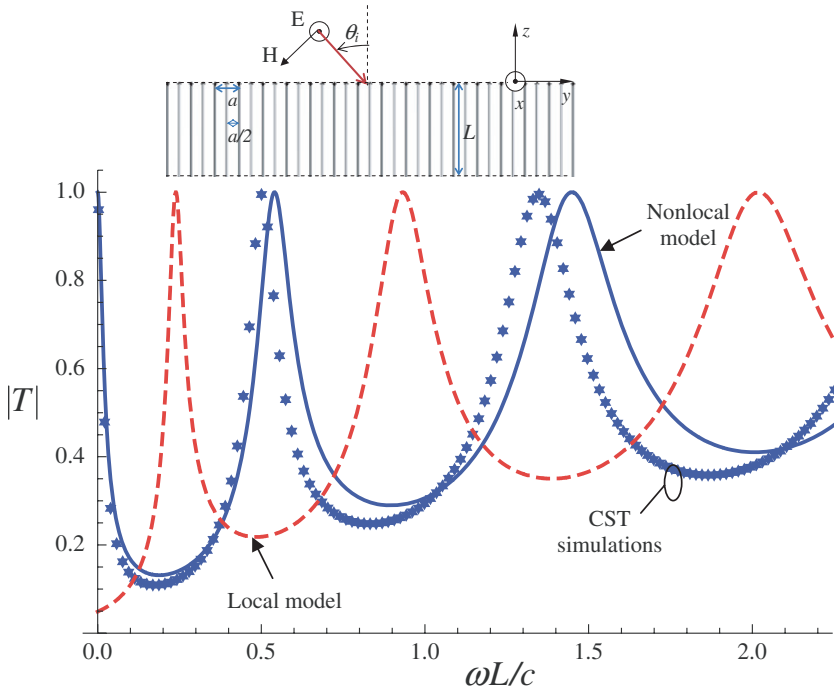

Figure 3. Magnitude of the transmission coefficient as a function of frequency for a metamaterial slab with a lattice constant $a = L/15$ and $r_w = 0.05a$ and a fixed thickness L. The solid line represents the spatially dispersive (nonlocal) model, the dashed line represents the local model. The discrete symbols were calculated with CST Microwave Studio. The inset shows the geometry of the problem.

The electric field in the air regions (below and above the metamaterial slab) can also be written as a superposition of (free-space) plane waves. By enforcing the continuity of the tangential components of the electric and magnetic field and the ABC (28) it is possible to determine the reflection and transmission coefficients for plane-wave incidence. For further details the reader is referred to [27] (in particular, formula (5) of [27] gives a closed form expression for the transmission coefficient T).

In the first example, we consider a metamaterial slab formed by PEC wires where the spacing between the wires is $a = L/15$ and L is the thickness of the slab. The host material is air. The amplitude of the transmission coefficient for plane-wave incidence along $\theta_i = 0.1^\circ$ is plotted in figure 3 as a function of the normalized frequency. It is seen that the results obtained with the nonlocal homogenization model and the proposed ABCs (solid line) compare well with the results obtained with the full-wave electromagnetic simulator CST Microwave Studio (discrete symbols) [42].

As mentioned before, in the absence of loss, the propagation constant $k_{z,(1)}$ may be assumed to be real valued (associated with a propagating mode in the wire medium), whereas the propagation constant of $k_{z,(2)}$ is purely imaginary (associated with an evanescent mode). Thus, it might be thought that this latter evanescent mode would play a minor role in the response of the metamaterial slab. In order to test this hypothesis, we have calculated the transmission coefficient obtained by setting $A_2^{\pm} = 0$ in equation (30). This condition removes the extra degree

of freedom of the problem, and thus to calculate the transmission coefficient it is sufficient to impose the classical boundary conditions at the interfaces, i.e. if one neglects the effect of the evanescent wave it is not necessary to consider an ABC at the interfaces. We refer to the results obtained with this approximation as the 'local model' results. A bit surprisingly, as reported in figure 3, the results obtained with the local model (dashed line) are qualitatively very different from the results obtained with the nonlocal model. In particular, the frequencies for which the local model predicts the maxima of T correspond to the minima of the nonlocal model, and vice versa. This demonstrates that the effect of the evanescent mode and the ABCs cannot be neglected, and they are essential to describe accurately the response of the material. It should be noted that the evanescent mode, even though strongly attenuated in the interior of the metamaterial slab, may be excited in the close vicinity of the interfaces in order to ensure that the microscopic current in the metallic wires vanishes at the interfaces. Thus, even though the wave propagation in the interior of the slab is dominated by the propagating mode, the 'effective wave impedance' at the interfaces is determined by both the propagating and the evanescent modes. This explains the disagreement between the local and nonlocal models reported in figure 3.

One of the interesting properties of the crossed wire mesh is that it may interact very strongly with the incoming wave, even when the length of the metallic wires is electrically short, effectively behaving as a material with very large dielectric constant [27]. For instance, in the example depicted in figure 3 the first dip of the transmission coefficient occurs for $\omega L/c \approx 0.2$, which corresponds to the metallic wires with length $L_w = \sqrt{2}L = 0.04\lambda_0$. This value is one order of magnitude smaller than the traditional $\lambda_0/2$ resonance of a metallic wire. Moreover, as discussed in [27], the resonance length of the wires may be made arbitrarily small by increasing the density of wires (number of wires per unit of volume), keeping the metal volume fraction unchanged. Indeed, unlike conventional metamaterial designs, the effective index of refraction of the material does not saturate when the inclusions are scaled and the lattice constant a is made smaller.

To further clarify these ideas we consider the scenarios depicted in figure 4. In panels (a) and (b), we represent a conventional metamaterial slab (e.g. an array of metal or dielectric spheres) with fixed thickness L, but different lattice constants a_x. The volume fraction of the inclusions is assumed to be the same in the two cases. Each inclusion is entirely contained in a basic cell. The incoming wave illuminates the slab along the normal direction. From the classical Clausius–Mossotti formula [43], it should be clear that in the quasi-static limit the value of the index of refraction of the bulk metamaterial will eventually saturate and become independent of the lattice constant a_x, when a_x is made sufficiently small (keeping the volume fraction of the inclusions unchanged). In fact, for a fixed frequency, and with a_x increasingly small, the index of refraction will obviously converge to the static case value. In particular, it is expected that in the quasi-static limit the transmission coefficient in configurations (a) and (b) will become independent of a_x, provided a_x is sufficiently small.

The situation for a crossed wire mesh is completely different. As discussed in section 4—see equation (25)—for a fixed frequency and a fixed metal volume fraction, the index of refraction of the bulk wire mesh can be made arbitrarily large by reducing the lattice constant a_x. Thus, despite the fact that the volume fraction of the metal is kept constant, the response of the structures depicted in figure 4(c) and (d) may be radically different. In particular, unlike in a conventional metamaterial, the response does not saturate when a_x is made increasingly small. This important qualitative difference between the wire mesh and a conventional metamaterial stems from the fact that in a wire mesh each inclusion is spanned over many unit cells, i.e. each

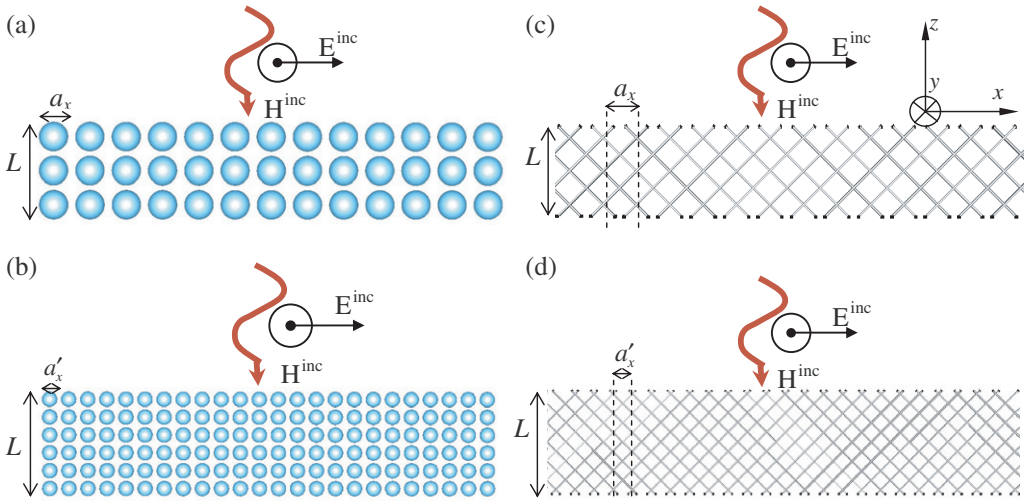

Figure 4. (a) generic metamaterial slab formed by inclusions whose size is smaller than the lattice constant. (c) crossed wire mesh slab formed by inclusions that are spanned over many unit cells. As discussed in the main text, unlike a standard metamaterial, the response of the crossed wire mesh does not saturate when the density of inclusions (number of inclusions per unit of volume) is increased, keeping the volume fraction constant (panels (b) and (d)).

individual wire crosses several unit cells (see figures 4(c) and (d) and its length is independent of the size of the cell. Obviously, this property precludes the application of the Clausius–Mossotti formula, and clarifies the strong coupling between the different inclusions and the anomalous electrical response of the wire mesh.

To illustrate how the response of the wire mesh is modified when the density of wires is increased, we have calculated the dispersion characteristic of the guided modes supported by the metamaterial slab (i.e. the waves that may propagate along the y-direction attached to the interfaces, even in the absence of an external source). The dispersion characteristic of the guided modes, $k_y = k_y(\omega)$, may be obtained from the poles of the transmission coefficient for plane-wave incidence [27].

In figure 5, we depict (solid lines) the calculated dispersion characteristics for a slab with thickness L and different values of the lattice constant a. The metal volume fraction is constant in all the examples ($r_w = 0.05a$). The results were obtained using the homogenization model. As with a conventional dielectric substrate, the crossed wire mesh supports a guided mode with no cut-off frequency, i.e. for arbitrarily long wavelengths. Consistent with the previous discussions, it can be seen that for a fixed frequency the effective index of refraction of the guided mode, $k_y c/\omega$, increases significantly when the lattice constant a is reduced from $a = L/5$ to $L/15$, i.e. when the density of the wires is increased. This simple example illustrates how, unlike with a conventional metamaterial slab, the response of the crossed wire mesh does not saturate as the lattice constant is made smaller.

Even though, for simplicity, the examples considered here assume PEC wires, the proposed homogenization model can also be applied when either the effect of loss or the plasmonic response of the metal is taken into account. For further details, the reader is referred to [27], where the model has been validated against full-wave simulations in such scenarios.

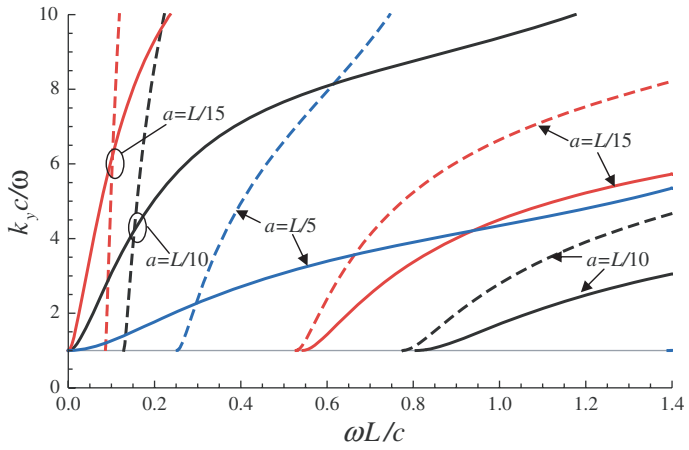

Figure 5. Dispersion characteristic of surface waves for a metamaterial slab with thickness L and different values of the lattice constant a. The radius of the wires is $r_w = 0.05a$. Solid lines: metamaterial slab stands in free-space. Dashed lines: grounded metamaterial slab.

5.2. Grounded slab

Next, we consider the case in which the bottom face of the metamaterial slab is covered with a metallic plane [14]. It is supposed that the metallic wires are attached to the ground plane with good Ohmic contact. In this configuration, assuming plane-wave incidence with the electric field polarized along the x-direction, the electric field inside the metamaterial slab can still be written as in equation (30). The boundary conditions at the air interface are the same as in section 5.1. On the other hand, at the metallic interface E_x must vanish, and the ABC (29) must be enforced. Proceeding in this manner (see [14]), it may be proven that the reflection coefficient referred to the air interface is

$$\rho = -1 + \frac{2\gamma_0 \left(k_{z,(2)}^2 - k_{z,(1)}^2\right)}{D(\omega, k_y)} \left[k_{z,(2)} \left(\gamma_h^2 + k_{z,(2)}^2\right) \tan(k_{z,(1)} L) - k_{z,(1)} \left(\gamma_h^2 + k_{z,(1)}^2\right) \tan(k_{z,(2)} L)\right] \tag{31}$$

$$\begin{aligned} D(\omega, k_y) = {} & k_{z,(1)} k_{z,(2)} \left[2\gamma_h^2 \left(\gamma_h^2 + k_{z,(1)}^2 + k_{z,(2)}^2\right) + k_{z,(1)}^4 + k_{z,(1)}^4\right] \\ & + \left(\gamma_h^2 + k_{z,(1)}^2\right) \left(\gamma_h^2 + k_{z,(2)}^2\right) \left[\left(k_{z,(1)}^2 + k_{z,(2)}^2\right) \tan(k_{z,(1)} L) \tan(k_{z,(2)} L) \right. \\ & \left. - 2k_{z,(1)} k_{z,(2)} \sec(k_{z,(1)} L) \sec(k_{z,(2)} L)\right] + \gamma_0 \left(k_{z,(2)}^2 - k_{z,(1)}^2\right) \\ & \times \left[k_{z,(2)} \left(\gamma_h^2 + k_{z,(2)}^2\right) \tan(k_{z,(1)} L) - k_{z,(1)} \left(\gamma_h^2 + k_{z,(1)}^2\right) \tan(k_{z,(2)} L)\right]. \end{aligned} \tag{32}$$

In equations (31) and (32), $k_{z,(1)}$ and $k_{z,(2)}$ are defined as in section 5.1, L is the thickness of the slab, $\gamma_0 = \sqrt{k_y^2 - \omega^2 \varepsilon_0 \mu_0}$, $\gamma_h = \sqrt{k_y^2 - \omega^2 \varepsilon_0 \mu_0 \varepsilon_h}$, and k_y is the transverse wavenumber of the incoming wave.

To illustrate the application of the formula, we have calculated the phase of the reflection coefficient as a function of frequency for a grounded metamaterial slab such that $a = L/10$ and different incidence angles. The wires are assumed to be perfect conductors and thus the

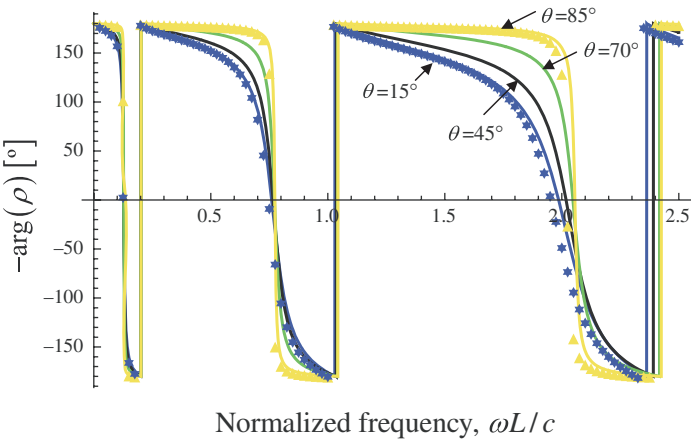

Figure 6. Phase of the reflection coefficient as a function of the normalized frequency for different angles of incidence. The lattice constant is $a = L/10$ and the radius of the wires is $r_w = 0.05a$, where L is the thickness of the grounded slab. The host material is air. Solid lines: homogenization model. Star- and triangle-shaped symbols: full-wave simulations for $\theta = 15^\circ$ and 85°, respectively.

magnitude of ρ is unity. The results obtained with equation (31) are depicted in figure 6 (solid lines) superposed on data obtained using CST Microwave Studio (discrete symbols) [42]. An excellent agreement is revealed supporting the validity of the proposed homogenization method. It is interesting to note that the frequencies where the phase of ρ vanishes are nearly independent of the angle of incidence. Thus, at such frequencies the grounded slab may mimic very closely the behavior of an ideal perfect magnetic conductor [44]. Moreover, due to the large index of refraction of the wire mesh such behavior may be obtained with a strongly subwavelength slab. For example, the first resonance in the example of figure 6 occurs for $L = 0.02\lambda_0$.

We have also calculated the dispersion characteristic $k_y = k_y(\omega)$ of the guided modes supported by the grounded slab. The dispersion characteristic is obtained by numerically solving the equation $D(\omega, k_y) = 0$ with respect to k_y, where $D(\omega, k_y)$ is defined by equation (32). The calculated results for a slab with fixed thickness L and different values of the lattice constant are depicted in figure 5 (dashed lines). Consistent with the results reported in [14] and the discussion of section 5.1, it is seen that when the density of wires is increased (i.e. a is reduced) the guided mode becomes more attached to the metamaterial slab. Unlike the case where the slab stands in free-space, the guided modes can only propagate above a certain cut-off frequency. Despite that, due to the anomalously high index of refraction of the crossed wire mesh, the metamaterial slab thickness may be strongly subwavelength at the onset of propagation of the fundamental mode [14, 26]. For example, for $a = L/10$ the thickness of the slab at the cut-off frequency of the fundamental mode is as small as $L = 0.02\lambda_0$. Thus, the proposed structure may enable the realization of ultra-subwavelength waveguides, as demonstrated experimentally in [26].

It should be mentioned that, unlike a conventional dielectric slab, the dispersion characteristic of a grounded crossed wires slab cannot be obtained from the dispersion characteristic of a slab standing in free-space. In fact, it is impossible to place a PEC plane

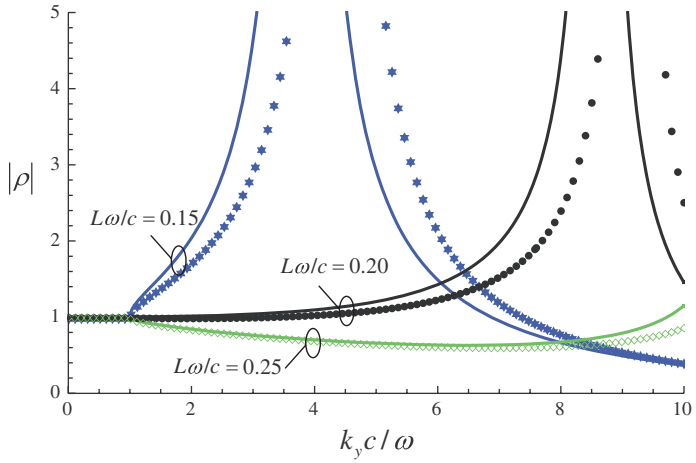

Figure 7. Amplitude of the reflection coefficient as a function of the transverse component of the wave vector k_y, and different frequencies of operation ω. The lattice constant is $a = L/10$ and the radius of the wires is $r_w = 0.05a$, where L is the thickness of the grounded slab. Solid lines: homogenization model. Discrete symbols: full-wave simulations.

at the mid-plane of a crossed wires slab standing in free-space without disturbing the fields, because the crossed wire mesh is not transformed into itself after reflection with respect to the xoy-plane.

We have used CST Microwave Studio, in order to partially validate the dispersion characteristics depicted in figure 5, obtained using the homogenization model. Assuming plane-wave incidence, we have calculated the amplitude of the reflection coefficient as a function of the transverse wavenumber of the incoming wave k_y, for several fixed frequencies (figure 7). For $k_y < \omega/c$ the incoming wave is a propagating wave ($k_y = \omega/c \sin\theta_i$), and, due to the conservation of energy, the reflection coefficient amplitude is unity. On the other hand, for $k_y > \omega/c$ the incoming wave is an evanescent mode, and thus (since an evanescent wave does not carry power), $|\rho|$ may be any nonnegative value, even larger than unity. Indeed, it should be clear from equation (31), that the points k_y associated with the dispersion characteristic of the guided modes correspond to the poles of the reflection coefficient. As seen in figure 7, there is good agreement between the response to evanescent waves predicted by the homogenization model (solid lines), and the actual response calculated using CST Microwave Studio (discrete symbols). In particular, the position of the poles is predicted with good accuracy, and thus these results partially validate the dispersion characteristic associated with $a = L/10$ (dashed line) in figure 5.

6. Propagation in the *xoz*-plane

Here, we discuss the application of the proposed ABCs to the case where the plane of incidence is the xoz-plane (figure 2(b)). The geometry of the double-wire medium slab is as explained in section 4. It is assumed that the incoming plane wave has parallel polarization (i.e. the electric field is in the xoz-plane, whereas the incident magnetic field is along the y-direction).

6.1. Slab standing in free-space

Considering the geometry of the system under study and the polarization of the incoming wave, it is obvious that the magnetic field in all space has a single Cartesian component, H_y. As in section 5.1, it is assumed that inside the metamaterial slab the field is written in terms of a superposition of plane waves. The propagation constants along z of the plane waves can be calculated by solving the dispersion characteristic (26) with respect to k_z, for a fixed frequency ω, and a fixed transverse wavenumber of the incident wave $k_x = \omega/c \sin\theta_\mathrm{i}$. It can be verified that the dispersion characteristic is equivalent to a polynomial equation of degree three in the variable k_z^2 [28]. Thus, the metamaterial slab supports three independent plane waves with the magnetic field along the y-direction. Clearly, this property is a consequence of the nonlocal effects, as in a local material two distinct plane waves (i.e. associated with different k_z^2) with the same magnetic field orientation cannot exist. The propagation constants along z of the plane waves in the bulk metamaterial are denoted by $k_{z,(1)}$, $k_{z,(2)}$ and $k_{z,(3)}$. Thus, the magnetic field inside the metamaterial slab ($-L < z < 0$) can be written as (the x-variation of the fields is suppressed),

$$H_y = A_1^+ \mathrm{e}^{+\mathrm{i}\,k_{z,(1)}z} + A_1^- \mathrm{e}^{-\mathrm{i}\,k_{z,(1)}z} + A_2^+ \mathrm{e}^{+\mathrm{i}\,k_{z,(2)}z} + A_2^- \mathrm{e}^{-\mathrm{i}\,k_{z,(2)}z} + A_3^+ \mathrm{e}^{+\mathrm{i}\,k_{z,(3)}z} + A_3^- \mathrm{e}^{-\mathrm{i}\,k_{z,(3)}z}, \quad -L < z < 0, \tag{33}$$

where $A_i^\pm$ are the complex amplitudes of the excited waves. For frequencies much lower than the plasma frequency of the wire medium, $\omega/c \ll \beta_\mathrm{p}/\sqrt{\varepsilon_\mathrm{h}}$, it can be verified that in the PEC case and for a propagating incoming wave, only a single propagation constant, let us say $k_{z,(1)}$, is real valued. The corresponding plane wave is associated with the hyperbolic isofrequency contours depicted in figure 2(b). The other two propagation constants, $k_{z,(2)}$ and $k_{z,(3)}$ are purely imaginary, and are associated with evanescent modes.

Assuming that the incoming plane wave propagates in the semi-space $z > 0$, the magnetic field in the air regions verifies

$$\begin{aligned} H_y &= H_y^\mathrm{inc}\left(\mathrm{e}^{\gamma_0 z} - \rho \mathrm{e}^{-\gamma_0 z}\right), \quad z > 0, \\ H_y &= H_y^\mathrm{inc} T \mathrm{e}^{\gamma_0 z}, \quad z < -L, \end{aligned} \tag{34}$$

where H_y^inc is the complex amplitude of the incident magnetic field, $\gamma_0 = -\mathrm{i}\sqrt{\omega^2\varepsilon_0\mu_0 - k_x^2} = \sqrt{k_x^2 - \omega^2\varepsilon_0\mu_0}$ is the propagation constant of the incoming wave along the z-direction, and ρ and T are the reflection and transmission coefficients, respectively.

The electrical field inside the metamaterial slab can be easily obtained from equation (33), by noting that for each individual plane wave of the type $\mathbf{H} = H_0 \mathrm{e}^{\mathrm{i}k_x x}\mathrm{e}^{\mathrm{i}\,k_z z}\hat{\mathbf{u}}_y$, the corresponding electric field is $\mathbf{E} = H_0\,\bar{\bar{\varepsilon}}^{-1} \cdot \left(\frac{k_z}{\omega\varepsilon_0}\hat{\mathbf{u}}_x - \frac{k_x}{\omega\varepsilon_0}\hat{\mathbf{u}}_z\right)\mathrm{e}^{\mathrm{i}k_x x}\mathrm{e}^{\mathrm{i}\,k_z z}$, where $\bar{\bar{\varepsilon}}^{-1}(\omega, \mathbf{k})$ is the inverse of the dielectric function of the crossed wire mesh, defined by equation (9) with $N = 2$. The averaged macroscopic current $\mathbf{J}_{d,\mathrm{av}}$ inside the metamaterial is finally obtained by replacing the electric field in formula (6), taking into account that for the present geometry $\mathbf{k}_\parallel = k_x\hat{\mathbf{u}}_x$. The formulae for $\mathbf{E}$ and $\mathbf{J}_{d,\mathrm{av}}$ are too long to show here, and thus are omitted.

As in section 5, the reflection and transmission coefficients can be calculated by imposing the continuity of the tangential electromagnetic fields (H_y and E_x components of the fields), and the two ABCs (7) ($N = 2$). Unlike in section 5, the two ABCs are not degenerate for the present geometry, and yield two independent equations. This property is consistent with the fact

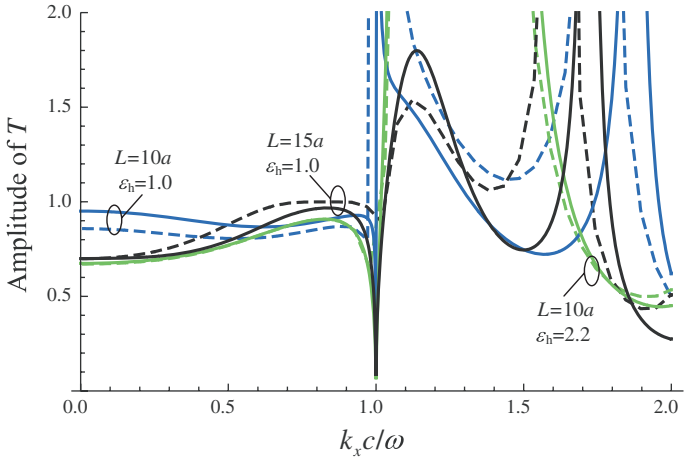

Figure 8. Amplitude of the transmission coefficient as a function of normalized k_x for a fixed frequency and different L and ε_h. The lattice constant is such that $\omega a/c = 0.6$, the radius of the wires is $r_w = 0.05a$. Solid lines: homogenization model. Dashed lines: full-wave simulations.

that the wire medium supports two additional waves for the present configuration, as is manifest from equation (33), and thus two ABCs are required to remove the two additional degrees of freedom.

We have applied the proposed homogenization procedure to characterize the response of a wire medium slab under plane-wave incidence. In figure 8, we depict the amplitude of the transmission coefficient, for a fixed frequency and lattice constant a, with $\omega a/c = 0.6$, and for different values of the slab thickness L, as a function of the transverse wavenumber k_x of the plane wave. As mentioned before $k_x = \omega/c \sin\theta_i$ for a propagating plane wave, whereas $k_x > \omega/c$ when the incoming wave is evanescent. For simplicity the wires are assumed to be perfect conductors. The results of figure 8 reveal a good agreement between the homogenization results (solid lines) and the full-wave simulations obtained with CST Microwave Studio (dashed lines), both for the propagating spectrum ($k_x < \omega/c$), and for the evanescent spectrum ($k_x > \omega/c$). The homogenization results are especially accurate in the example where the permittivity of the host material is $\varepsilon_h = 2.2$. It is seen that the transmission coefficient may have several poles, which indicates the presence of guided modes.

As reported in [28], as a consequence of the hyperbolic-shaped isofrequency contours associated with the propagating mode (figure 2(b)), the Poynting vector suffers negative refraction at the interface between a crossed wire mesh and air. Therefore, unlike in a conventional dielectric slab, the incident beam suffers a negative lateral shift Δ as it propagates through the wire medium slab [28] (the inset in figure 9 represents the case in which Δ is positive). As demonstrated in [28], the spatial shift Δ can be related to the phase $\phi = -\arg T$ of the transmission coefficient ($T = |T|e^{-i\phi}$), by the simple formula $\Delta = d\phi/dk_x$. Thus, the spatial shift is proportional to the slope of the phase of T. Hence, when ϕ is an increasing function of k_x the lateral shift is positive and the beam is positively refracted (this is what happens in a conventional dielectric slab). On the other hand, when ϕ is a decreasing function of k_x the lateral shift is negative, which indicates that the beam is negatively refracted [28].

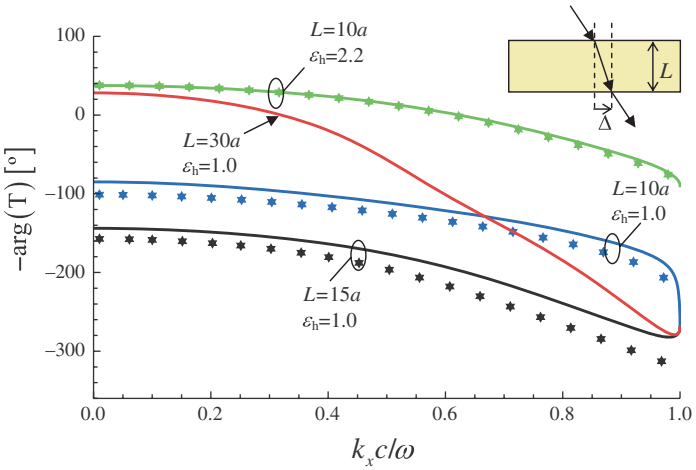

Figure 9. Phase of the transmission coefficient as a function of normalized k_x for a fixed frequency and different L and ε_h. The lattice constant is such that $\omega a/c = 0.6$, the radius of the wires is $r_w = 0.05a$. Solid lines: homogenization model. Dashed lines: full-wave simulations.

In order to show that our homogenization model predicts the emergence of negative refraction, we have calculated the phase of the transmission coefficient as a function of $k_x = \omega/c \sin\theta_i$, for the normalized frequency $\omega a/c = 0.6$ (ω and a are fixed). The obtained results are represented in figure 9 for different thicknesses of the metamaterial slab. The discrete symbols were calculated using CST Microwave Studio. It is seen in figure 9 that, consistent with the results reported in [28], the phase ϕ is indeed a decreasing function of k_x. In particular, it is seen that for thicker slabs the slope of ϕ becomes more negative, which indicates, as could be expected, that the lateral spatial shift becomes larger. Similarly, the slope also increases with the angle of incidence (i.e. with k_x), consistent with the fact that for larger values of θ_i the beam is more refracted at the interface [28]. As demonstrated in [28], the phenomenon of negative refraction is very broadband.

6.2. Grounded slab

For the sake of completeness, we have also studied the application of the ABCs to the case where the bottom face of the metamaterial slab is grounded ($z = -L$). As in section 6.1, the magnetic field inside the wire medium is written as in equation (33). The magnetic field in the air region ($z > 0$) is defined in the same manner as in equation (34). For this configuration, the homogenization procedure is similar to that described in section 6.1, except that at the ground plane it must be enforced that $E_x = 0$ and the two ABCs (8) ($N = 2$). We have applied this analytical formalism to characterize the electromagnetic response (under plane-wave incidence) of a grounded metamaterial slab with a fixed thickness L and the lattice constant $a = L/10$ as a function of frequency. In figure 10, we depict the reflection coefficient phase (solid lines) calculated for different angles of incidence. The host material is air and the wires are perfect conductors. Similar to the results of section 5.2, it is seen that at certain frequencies, nearly independent of the angle of incidence, the metamaterial may behave as a high-impedance ground plane, and mimic very closely the behavior of a perfect magnetic

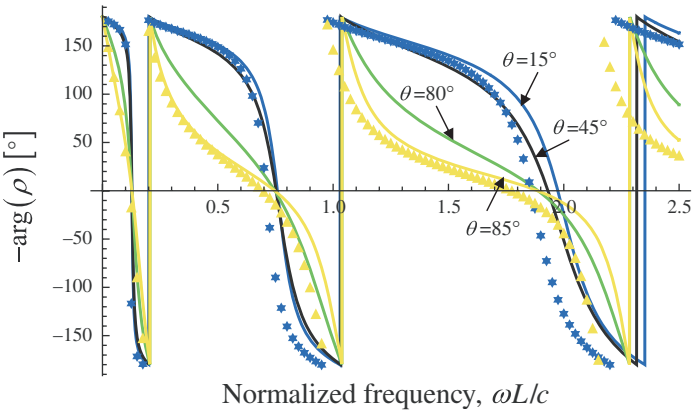

Figure 10. Phase of the reflection coefficient as a function of the normalized frequency for different angles of incidence. The lattice constant is $a = L/10$ and the radius of the wires is $r_w = 0.05a$, where L is the thickness of the grounded slab. Solid lines: homogenization model. Star- and triangle-shaped symbols: full-wave simulations for $\theta = 15^\circ$ and 85°, respectively.

conductor. It should be noted that in the present configuration the incoming wave is TM-polarized, whereas in section 5.2 the wave is TE polarized. Thus, the high-impedance property is independent of the polarization. The homogenization results agree well with the full-wave simulations computed with CST Microwave Studio (discrete symbols), which further validates our homogenization theory.

7. Conclusion

We extended our previous work on ABCs [35, 36] to wire media formed by N different nonconnected components ($N = 1, 2, 3$). Using simple physical arguments, it was demonstrated that in general N different ABCs must be considered at an interface. These ABCs were derived for cases where the wire medium is adjacent to either a dielectric or a conducting material. It was proven that in the absence of loss the proposed ABCs ensure the conservation of the power flow, and in particular a general formula was derived for the Poynting vector in the wire medium. We have illustrated the application of the proposed ABCs when the metamaterial is formed by a double array of metallic wires ($N = 2$). It was demonstrated that the proposed homogenization concepts enable the accurate numerical modeling of the considered nonlocal materials in scattering problems (for both propagating and evanescent incident waves) and in propagation problems (calculation of the guided modes). In particular, we have highlighted the anomalous physical properties of nonconnected wire media, and demonstrated that these materials may permit the construction of very compact devices as well as the emergence of negative refraction.

Acknowledgments

This work is supported in part by Fundação para a Ciência e a Tecnologia as project PDTC/EEA-TEL/71819/2006.

Appendix A

In this appendix, we demonstrate that in nonconnected wire media the bulk macroscopic fields may be accurately approximated with the TA fields, provided none of the unit vectors $\hat{\mathbf{u}}_n$ lies in the transverse (xoy) plane. This result is a generalization taken from a property characteristic of arrays of parallel wires and applied to double- and triple-wire media [36].

To this end, we consider the unbounded periodic material, making an assumption that the microscopic fields $(\mathbf{e}, \mathbf{b})$ have the Floquet–Bloch property, i.e. $(\mathbf{e}, \mathbf{b})\mathrm{e}^{-\mathrm{i}\mathbf{k}\cdot\mathbf{r}}$ has the same translational symmetry as the lattice, where $\mathbf{k}$ is the associated wave vector. Following [18, 37] the bulk electric field is defined by $\mathbf{E} = \mathbf{E}_{\mathrm{av}}\mathrm{e}^{\mathrm{i}\mathbf{k}\cdot\mathbf{r}}$ with (using the time convention $\mathrm{e}^{-\mathrm{i}\omega t}$):

$$\mathbf{E}_{\mathrm{av}} = \frac{1}{\mathrm{V}_{\mathrm{cell}}}\int_{\Omega}\mathbf{e}(\mathbf{r})\mathrm{e}^{-\mathrm{i}\mathbf{k}\cdot\mathbf{r}}\mathrm{d}^3\mathbf{r}. \tag{A.1}$$

The macroscopic induction field $\mathbf{B}_{\mathrm{av}}$ is defined similarly. In the above, Ω represents the unit cell of the nonconnected wire medium, and $V_{\mathrm{cell}} = a^3$ is its volume. The bulk macroscopic fields verify the system [18, 37]

$$\begin{aligned}\mathrm{i}\mathbf{k}\times\frac{\mathbf{B}_{\mathrm{av}}}{\mu_0} &= -\mathrm{i}\omega\varepsilon_0\varepsilon_{\mathrm{h}}\mathbf{E}_{\mathrm{av}} - \mathrm{i}\omega\mathbf{P}_{\mathrm{av}},\\ \mathrm{i}\mathbf{k}\times\mathbf{E}_{\mathrm{av}} &= \mathrm{i}\omega\,\mathbf{B}_{\mathrm{av}},\end{aligned} \tag{A.2}$$

where the generalized polarization vector, $\mathbf{P}_{\mathrm{av}}$, is given by

$$\mathbf{P}_{\mathrm{av}} = \frac{1}{-\mathrm{i}\omega\mathrm{V}_{\mathrm{cell}}}\int_{\partial D}\mathbf{J}_{\mathrm{c}}(\mathbf{r})\mathrm{e}^{-\mathrm{i}\,\mathbf{k}\cdot\mathbf{r}}\mathrm{d}s \tag{A.3}$$

and $\mathbf{J}_{\mathrm{c}}$ is the density of current over the surface ∂D of the metallic wires enclosed in the unit cell. The dielectric function of the bulk material (defined by equation (9)) is such that $\bar{\bar{\varepsilon}}(\omega, \mathbf{k})\cdot\mathbf{E}_{\mathrm{av}} = \varepsilon_0\varepsilon_{\mathrm{h}}\mathbf{E}_{\mathrm{av}} + \mathbf{P}_{\mathrm{av}}$ [18].

The objective here is to relate the bulk medium fields with the TA fields defined by (1). Note that unlike with the bulk medium fields, the definition of the TA fields depends on the considered transverse plane or, equivalently, depends on the orientation of the wires relative to the transverse plane (which is assumed in this work to be the xoy-plane). We suppose that the transverse unit cell Ω_{T} may be related to the unit cell of the bulk material as, $\Omega = \Omega_{\mathrm{T}}\times[-a_z/2, a_z/2]$ for some a_z, which may depend on the orientation of the wires relative to the transverse plane. From equation (26) of [37] it is known that the generalized polarization vector may be written as a function of the TA density of current as

$$\mathbf{P}_{\mathrm{av}} = \frac{1}{-\mathrm{i}\omega a_z}\int_{-a_z/2}^{a_z/2}\mathbf{J}_{d,\mathrm{av}}(z)\mathrm{e}^{-\mathrm{i}k_z z}\mathrm{d}z, \tag{A.4}$$

where k_z is the z-component of the wave vector. But, as demonstrated in section 2, within the thin-wire approximation, the TA current is expressed in terms of the microscopic currents as in equation (5). Moreover, since we assume here that the microscopic fields verify the Floquet–Bloch condition (along three independent directions of space) it is clear that the microscopic currents must be such that $I_n(z) = I_n\mathrm{e}^{\mathrm{i}k_z z}$, for some I_n. Taking this property into account, and using equation (5), it is apparent that equation (A.4) implies that

$$\mathbf{J}_{d,\mathrm{av}}(z) = -\mathrm{i}\omega\mathbf{P}_{\mathrm{av}}\mathrm{e}^{\mathrm{i}k_z z}. \tag{A.5}$$

Therefore, within the thin-wire approximation, and independent of the orientation of the wires relative to the interface, the TA current associated with a Floquet mode of the unbounded material can be written in terms of the polarization vector of the bulk material as in equation (A.5). This result implies that the TA fields must verify

$$\mathbf{E}_{\mathrm{av,T}}(z) = \mathbf{E}_{\mathrm{av}}\, \mathrm{e}^{\mathrm{i}k_z z}, \quad \mathbf{B}_{\mathrm{av,T}}(z) = \mathbf{B}_{\mathrm{av}}\, \mathrm{e}^{\mathrm{i}k_z z}. \tag{A.6}$$

Indeed, in the considered scenario the TA fields are univocally determined by the (k_z-Floquet) solution of the differential system (2) with $\mathbf{J}_{d,\mathrm{av}}$ given by equation (A.5). But since the bulk medium fields verify equation (A.2), and noting that the wave vector can be decomposed as $\mathbf{k} = \mathbf{k}_{\parallel} + k_z \hat{\mathbf{u}}_z$, $\mathbf{k}_{\parallel}$ being the projection of the wave vector into the transverse plane, it readily follows that the solution of the differential system (2) is given by (A.6). This demonstrates that the TA fields can be identified with the bulk medium fields, as we wanted to show. It should also be clear that equation (A.6) can be immediately generalized to the case where the microscopic fields are a superposition of several Floquet–Bloch modes (associated with different wave vectors). In this case, the TA fields are obviously given by a superposition of plane waves (each plane wave being associated with a different Floquet mode as in equation (A.6)).

As a final remark, we note that the result (A.6) is only valid if there are no wires parallel (or quasi-parallel) to the interface because, as noted in section 2, equation (3) becomes singular in such circumstances. In fact, it was demonstrated in [37] that when some wires are parallel to the interface the TA fields cannot really be identified with the bulk macroscopic fields. The reader is referred to [37] for more details about the methods that can be used to study such configurations.

Appendix B

In this appendix, we demonstrate that for the superposition of plane waves (22), S_z defined by equation (19) may be written as in equation (23).

To begin with, we note that the polarization vector associated with the superposition of plane waves is

$$\mathbf{P}(\mathbf{r}) = \varepsilon_0 \sum_l \left(\bar{\bar{\varepsilon}}\,(\omega, \mathbf{k}_l) - \varepsilon_{\mathrm{h}} \bar{\bar{\mathbf{I}}} \right) \cdot \mathbf{E}_l \mathrm{e}^{+\mathrm{i}\mathbf{k}_l \cdot \mathbf{r}}, \tag{B.1}$$

where $\bar{\bar{\varepsilon}}$ is the dielectric function of the wire medium. In particular, the projection of $\mathbf{P}$ onto the direction $\hat{\mathbf{u}}_n$ (parallel to one of the wire arrays) verifies

$$P_n = \varepsilon_0 \sum_l \left(\varepsilon_{n,n}\,(\omega, \mathbf{k}_l) - \varepsilon_{\mathrm{h}} \right) \hat{\mathbf{u}}_n \cdot \mathbf{E}_l \mathrm{e}^{+\mathrm{i}\mathbf{k}_l \cdot \mathbf{r}} \tag{B.2}$$

and,

$$\left(\mathrm{i}\mathbf{k}_{\parallel} + \frac{\mathrm{d}}{\mathrm{d}z} \hat{\mathbf{u}}_z \right) \cdot \hat{\mathbf{u}}_n P_n = \varepsilon_0 \sum_l \left(i\mathbf{k}_l \cdot \hat{\mathbf{u}}_n \right) \left(\varepsilon_{n,n}(\omega, \mathbf{k}_l) - \varepsilon_{\mathrm{h}} \right) \hat{\mathbf{u}}_n \cdot \mathbf{E}_l \mathrm{e}^{+\mathrm{i}\mathbf{k}_l \cdot \mathbf{r}}. \tag{B.3}$$

On the other hand, explicit calculations show that

$$\left(\varepsilon_{n,n} - \varepsilon_{\mathrm{h}} \right)^{-1} \frac{\partial \varepsilon_{n,n}}{\partial k_z} = \frac{1}{\varepsilon_{\mathrm{h}} \beta_{\mathrm{p}}^2} \left(\varepsilon_{n,n} - \varepsilon_{\mathrm{h}} \right) \left(-2\mathbf{k} \cdot \hat{\mathbf{u}}_n \right) \left(\hat{\mathbf{u}}_z \cdot \hat{\mathbf{u}}_n \right). \tag{B.4}$$

Substituting equations (B.2)–(B.4) and equation (22) into equation (19), it is found that

$$S_z = S_z^0 - \frac{\omega}{4}\varepsilon_0 \sum_{l,m} \mathrm{Re}\left\{ \sum_{n=1}^{N} \left(\varepsilon_{n,n}(\omega, \mathbf{k}_l) - \varepsilon_\mathrm{h}\right)^{-1} \left(\varepsilon_{n,n}(\omega, \mathbf{k}_m) - \varepsilon_\mathrm{h}\right)^* \right.$$
$$\left. \times \mathbf{E}_m^* \cdot \hat{\mathbf{u}}_n \frac{\partial \varepsilon_{n,n}}{\partial k_z}(\omega, \mathbf{k}_l)\, \hat{\mathbf{u}}_n \cdot \mathbf{E}_l \mathrm{e}^{\mathrm{i}(\mathbf{k}_l - \mathbf{k}_m^*)\cdot\mathbf{r}} \right\}. \tag{B.5}$$

This result and the definition of S_z^0 (11) show that S_z may be written as a linear combination of exponentials of the type $\mathrm{e}^{\mathrm{i}(\mathbf{k}_l - \mathbf{k}_m^*)\cdot\mathbf{r}}$, where l and m identify a generic plane wave from the set considered. However, from equation (18) we know that in the lossless case S_z must be a constant, i.e. independent of $\mathbf{r}$. This means that in equation (B.5) the coefficients associated with the exponential $\mathrm{e}^{\mathrm{i}(\mathbf{k}_l - \mathbf{k}_m^*)\cdot\mathbf{r}}$ necessarily vanish when $\mathbf{k}_l \neq \mathbf{k}_m^*$. Hence, using the properties $\varepsilon_{n,n}(\omega, \mathbf{k}_m)^* = \varepsilon_{n,n}(\omega, \mathbf{k}_m^*)$ and $\frac{\partial \bar{\bar{\varepsilon}}}{\partial k_z} = \sum_{n=1}^{N} \frac{\partial \varepsilon_{n,n}}{\partial k_z} \hat{\mathbf{u}}_n \hat{\mathbf{u}}_n$, we finally conclude that S_z may be written as in equation (23).

References

[1] Pendry J, Holden A J, Stewart W J and Youngs I 1996 *Phys. Rev. Lett.* **76** 4773
[2] Smith D R, Padilla W, Vier D, Nemat-Nasser S and Schultz S 2000 *Phys. Rev. Lett.* **84** 4184
[3] Pokrovsky A L and Efros A L 2002a *Phys. Rev. Lett.* **89** 093901
[4] Belov P, Marqués R, Maslovski S, Nefedov I, Silveirinha M, Simovski C and Tretyakov S 2003 *Phys. Rev.* B **67** 113103
[5] Nefedov I S, Viitanen A J and Tretyakov S A 2005a *Phys. Rev.* B **72** 245113
[6] Nefedov I S, Viitanen A J and Tretyakov S A 2005b *Phys. Rev.* E **71** 046612
[7] Belov P A, Hao Y and Sudhakaran S 2006 *Phys. Rev.* B **73** 033108
[8] Shin J, Shen J and Fan S 2007 *Phys. Rev.* B **76** 113101
[9] Shvets G, Trendafilov S, Pendry J B and Sarychev A 2007 *Phys. Rev. Lett.* **99** 053903
[10] Ikonen P, Simovski C, Tretyakov S, Belov P and Hao Y 2007 *Appl. Phys. Lett.* **91** 104102
[11] Belov P A, Zhao Y, Tse S, Ikonen P, Silveirinha M G, Simovski C R, Tretyakov S, Hao Y and Parini C 2008 *Phys. Rev.* B **77** 193108
[12] Yao J, Liu Z, Liu Y, Wang Y, Sun C, Bartal G, Stacy A M and Zhang X 2008 *Science* **321** 930
[13] Liu Y, Bartal G and Zhang X 2008 *Opt. Express* **16** 15439
[14] Silveirinha M G and Fernandes C A 2008 *Phys. Rev.* B **78** 033108
[15] Silveirinha M G 2009a *Phys. Rev.* B **79** 035118
[16] Silveirinha M G 2006a *Phys. Rev.* E **73** 046612
[17] Pokrovsky A L and Efros A L 2002b *Phys. Rev.* B **65** 045110
[18] Silveirinha M G and Fernandes C A 2005 *IEEE Trans. Microw. Theory Tech.* **53** 1418
[19] Simovski C R and Belov P A 2004 *Phys. Rev.* E **70** 046616
[20] Shvets G 2002 CP647 *Advanced Accelerator Concept: Tenth Workshop* ed C E Clayton and P Muggli (American Institute of Physics) p 371
[21] Shapiro M A, Shvets G, Sirigiri J R and Temkin R J 2006 *Opt. Lett.* **31** 2051
[22] Pollard R J, Murphy A, Hendren W, Evans P, Atkinson R, Wurtz G A, Zayats A and Podolskiy V A 2009 *Phys. Rev. Lett.* **102** 127405
[23] Demetriadou A and Pendry J B 2008 *J. Phys.: Condens. Matter* **20** 295222
[24] Silveirinha M G, Belov P A and Simovski C R 2007 *Phys. Rev.* B **75** 035108
[25] Silveirinha M G, Belov P and Simovski C R 2008a *Opt. Lett.* **33** 1726
[26] Silveirinha M G, Fernandes C A, Costa J R and Medeiros C R 2008b *Appl. Phys. Lett.* **93** 174103
[27] Silveirinha M G, Fernandes C A and Costa J R 2008c *Phys. Rev.* B **78** 195121

[28] Silveirinha M G 2009b *Phys. Rev.* B **79** 153109
[29] Silveirinha M G 2009c *Phys. Rev. Lett.* **102** 193903
[30] Mahan G and Obermair G 1969 *Phys. Rev.* **183** 834
[31] Melnyk A R and Harrison M J 1970 *Phys. Rev.* B **2** 835
[32] Pekar S 1958 *Sov. Phys.—JETP* **6** 785
[33] Davis W A and Krowne C M 1998 *IEEE Trans. Antennas Propag.* **36** 97
[34] Henneberger K 1998 *Phys. Rev. Lett.* **80** 2889
[35] Silveirinha M G 2006b *IEEE Trans. Antennas Propag.* **54** 1766
[36] Silveirinha M G, Fernandes C A and Costa J R 2008d *New J. Phys.* **10** 053011
[37] Silveirinha M G and Fernandes C A 2007 *Phys. Rev.* E **75** 036613
[38] Landau L D, Lifshitz E and Pitaevskii L 2004 *Electrodynamics of Continuous Media* 2nd edn (Amsterdam: Elsevier)
[39] Agranovich V and Ginzburg V 1966 *Spatial Dispersion in Crystal Optics and the Theory of Excitons* (New York: Wiley Interscience)
[40] Shen J T, Catrysse P B and Fan S 2005 *Phys. Rev. Lett.* **94** 197401
[41] Shin J, Shen J-T and Fan S 2009 *Phys. Rev. Lett.* **102** 093903
[42] CST Microwave Studio 2008 CST GmbH http://www.cst.com
[43] Jackson J D 2001 *Classical Electrodynamics* 3rd edn (New York: Wiley)
[44] Sievenpiper D, Zhang L, Broas R, Alexopolous N and Yablonovitch E 1999 *IEEE Trans. Microw. Theory Tech.* **47** 2059